Supporting Information

Stacking engineering in two-dimensional multiferroic $CuInP_2S_6/CrI_3$ heterostructures

Yue Yang [a], Ying Zhao [a], Yan Su[a], Jijun Zhao[b,c], Xue Jiang*[b,c]

[a]*Key Laboratory of Materials Modification by Laser, Ion and Electron Beams (Ministry of Education), Dalian University of Technology, Dalian 116024, China.*

[b]*Guangdong Basic Research Center of Excellence for Structure and Fundamental Interactions of Matter, Guangdong Provincial Key Laboratory of Quantum Engineering and Quantum Materials, School of Physics, South China Normal University, Guangzhou 510006, China.*

[c]*Quantum Science Center of Guangdong-Hong Kong-Macao Greater Bay Area, Shenzhen-Hong Kong International Science and Technology Park, Shenzhen 518000, China.*

**Corresponding author E-mail: jiangx@scnu.edu.cn*

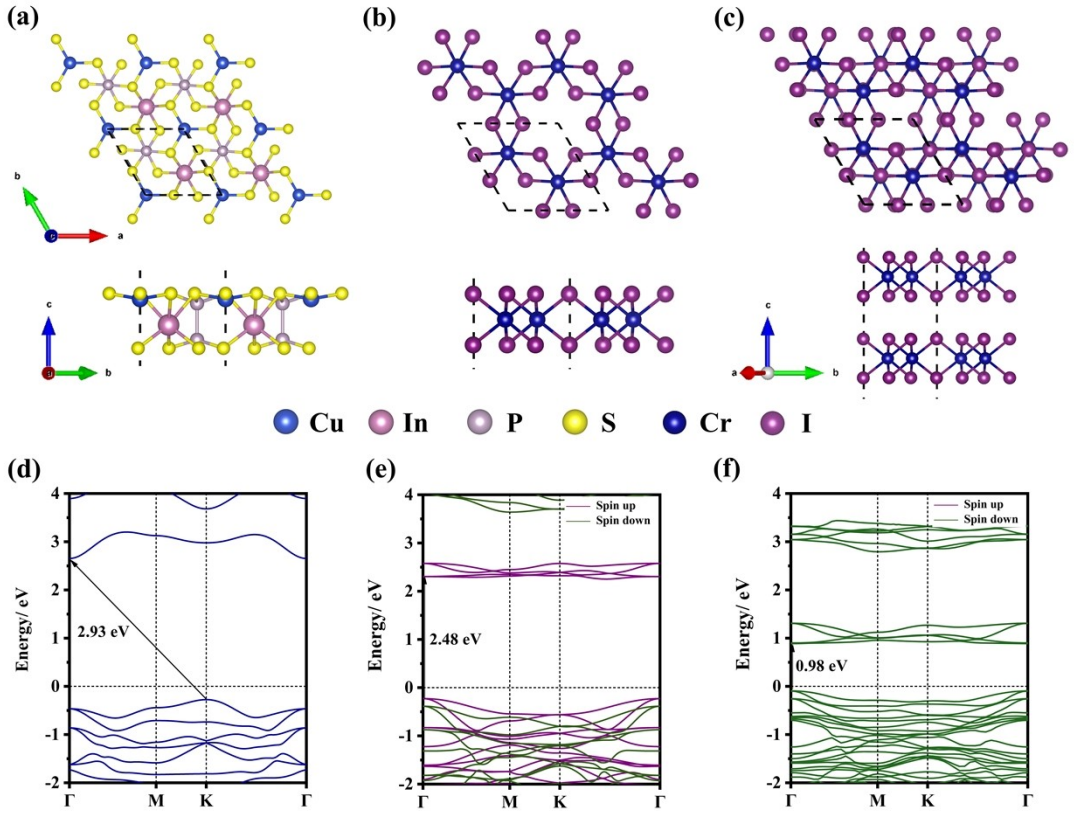

Figure S1. Top and side views of the (a) $CuInP_2S_6$ monolayer, (b) CrI_3 monolayer and (c) CrI_3 bilayer. The band structure of the (d) $CuInP_2S_6$ monolayer, (e) CrI_3 monolayer and (c) CrI_3 bilayer. The purple and green curves denote spin-up and spin-down bands, respectively.

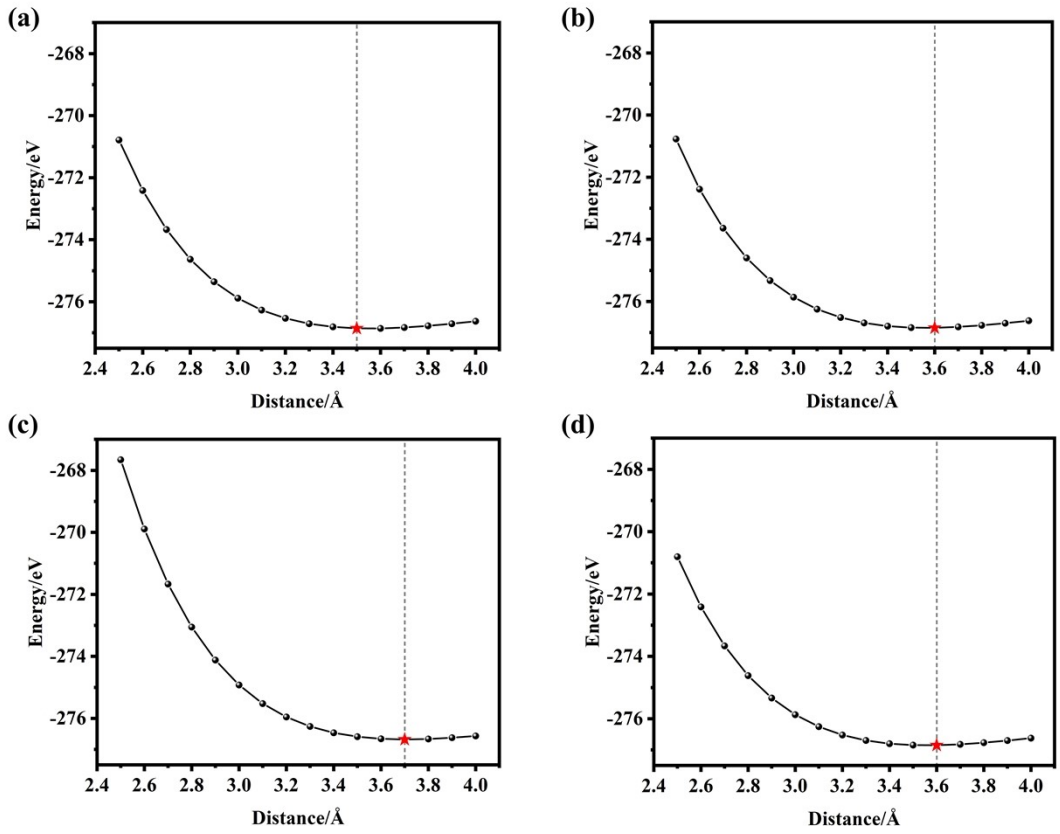

Figure S2. The energy of $CuInP_2S_6$/ monolayer-CrI_3 heterostructures with different stacking configurations — (a) stacking-I, (b) stacking-II, (c) stacking-III and (d) stacking-IV — as a function of the interlayer spacing. This is based on benchmark works before structural optimization. The dashed gray line indicates the lowest structural energy under this interlayer spacing.

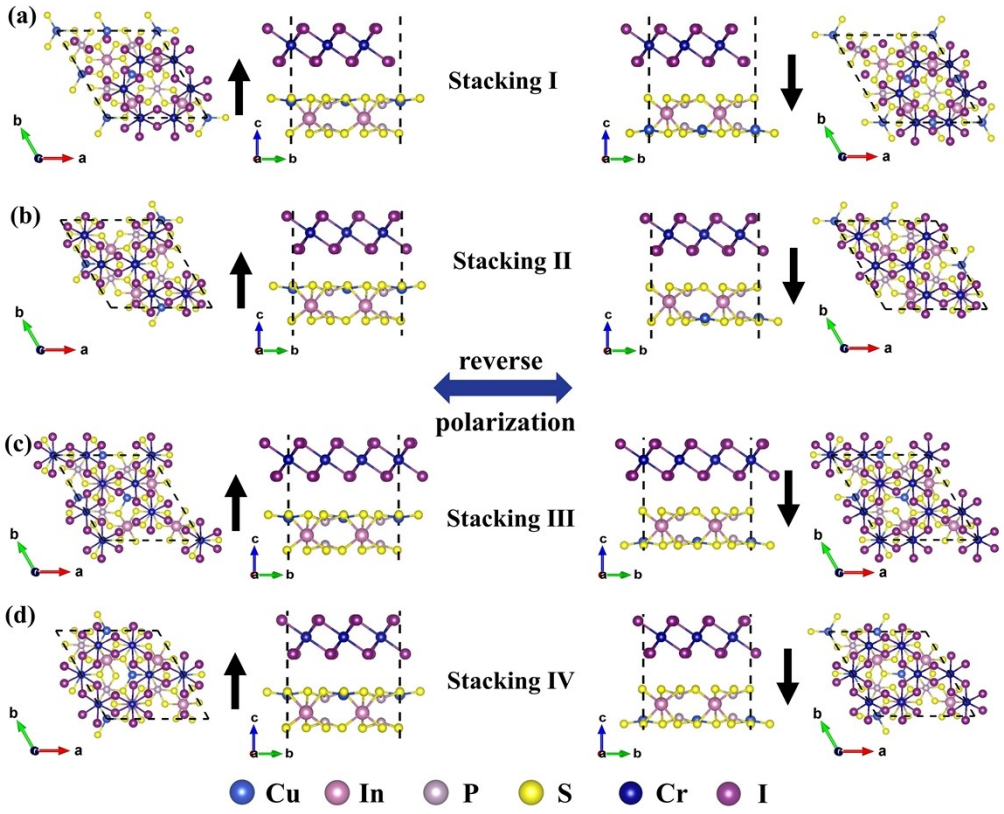

Figure S3. The top and side views of $CuInP_2S_6$/ monolayer-CrI_3 heterostructures with (a) stacking-I, (b) stacking-II, (c) stacking-III, and (b) stacking-IV. The black arrows show the direction of out-of-plane electric polarization.

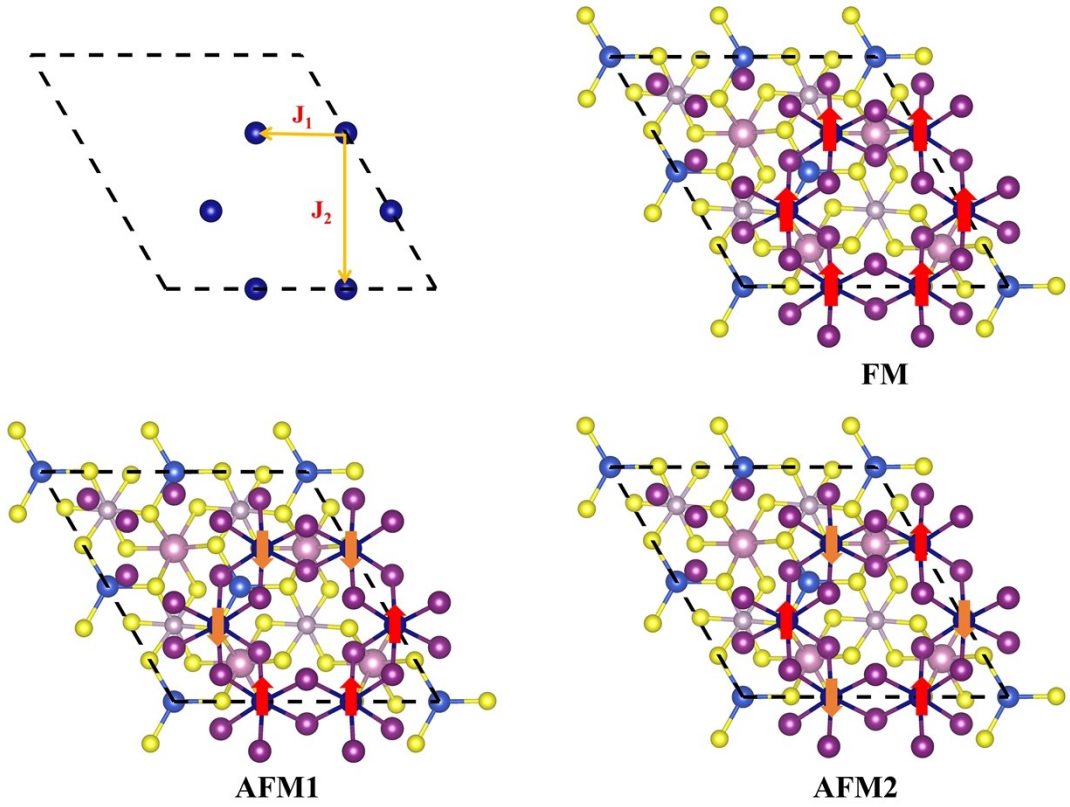

Figure S4. (a) Schematic diagrams of different magnetic coupling coefficient J for $CuInP_2S_6$/ monolayer-CrI_3 heterostructures (Only display Cr atoms). Schematic of FM (b), AFM1 (c) and AFM2 (d) of $CuInP_2S_6$/ monolayer-CrI_3 heterostructures. The spin orientations of the magnetic atoms are indicated by the arrows with different colors.

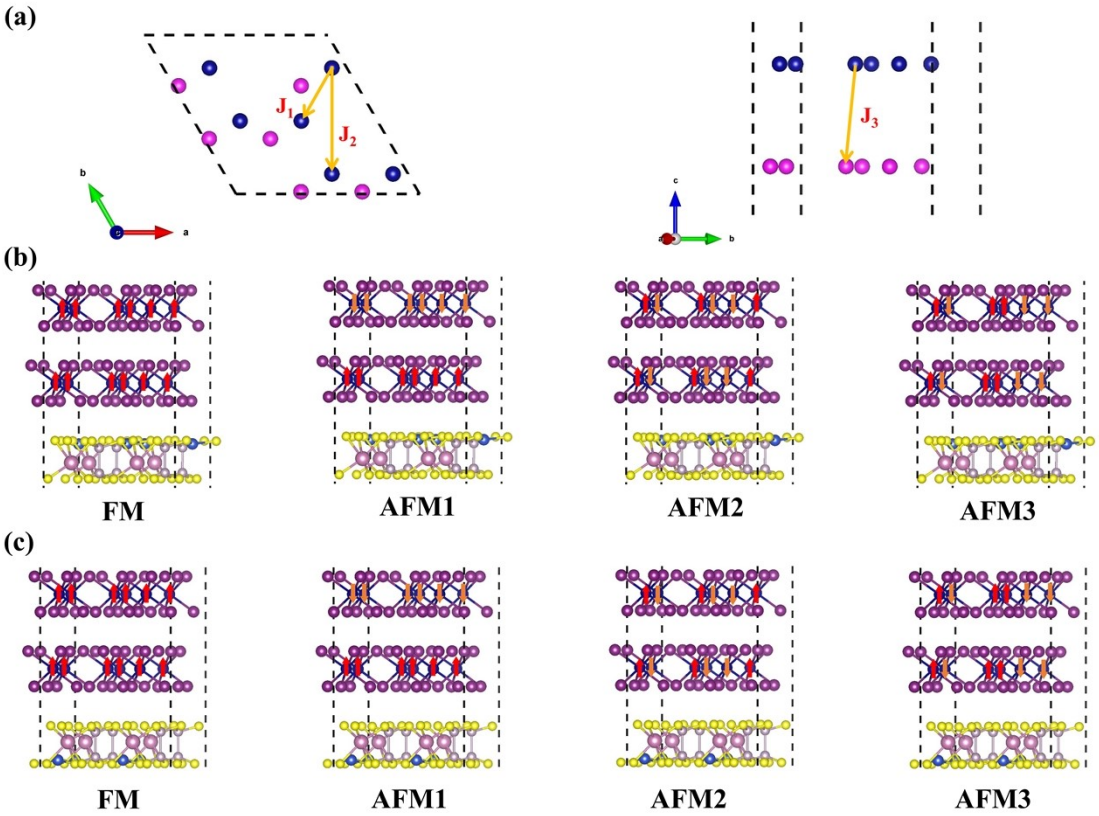

Figure S5. (a) Schematic diagrams of different magnetic coupling coefficient J for $CuInP_2S_6$/bilayer-CrI_3 heterostructures (Only display Cr atoms, blue and pink represent Cr atoms in the upper and lower layers, respectively). Side view of different magnetic configurations for $CuInP_2S_6$/bilayer-CrI_3 heterostructures in (b) upward and (c) downward polarizations. The spin orientations of the magnetic atoms are indicated by the arrows with different colours.

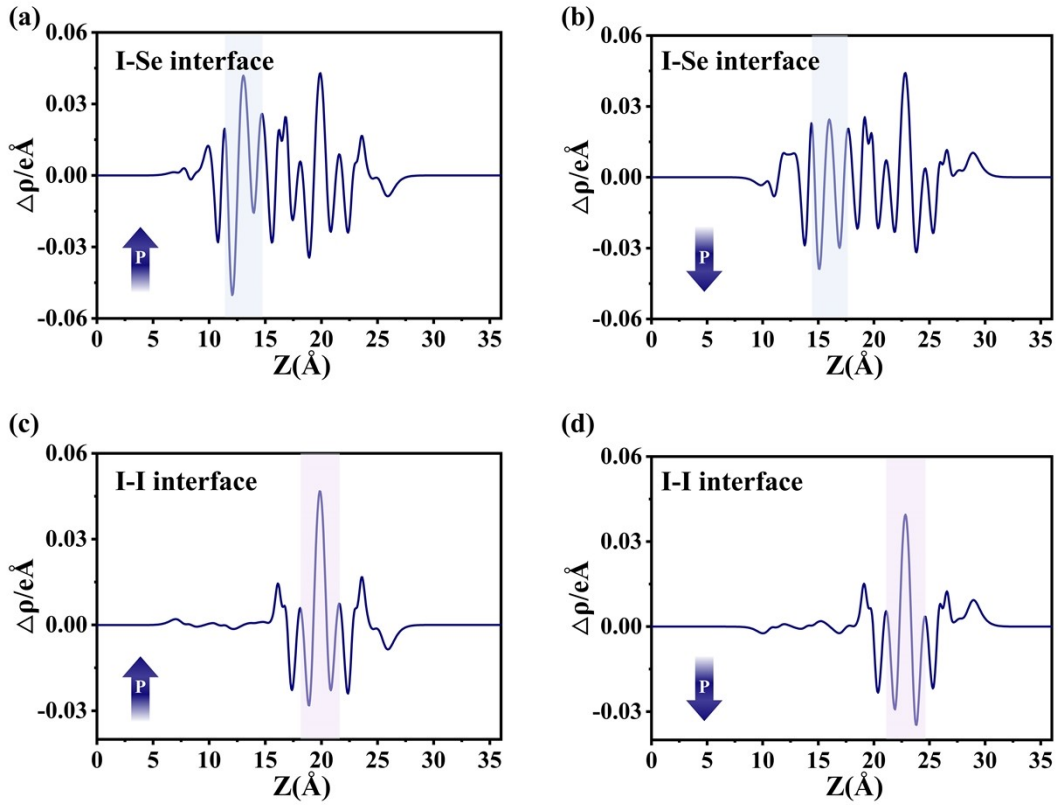

Figure S6. The planar-averaged charge density differences at I-Se interface (a), (b) and I-I interface (c), (d) for $CuInP_2S_6$/bilayer-CrI_3, respectively. Shaded region refers to the interface.

The exchange coupling strength J

The magnetic exchange parameters of $CuInP_2S_6$/bilayer-CrI_3 heterostructures are estimated through Heisenberg model:

$$H = -\sum_{ij} J_1 M_i M_j - \sum_{k,l} J_2 M_k M_l - \sum_{m,n} J_3 M_m M_n \quad \text{(S1)}$$

Where M is the magnetic moment of each Cr atom, J_1, J_2 and J_3 are the first-, second-and third-nearest-neighbor exchange parameters, respectively. Among them, J_1 and J_2 represent the intralayer coupling, while J_3 is the interlayer interactions, as shown in **Figure S5(a)**. These exchange parameters can be derived from the energy differences of the FM and four AFM configurations through the following equations:

$$E_{FM} = -(18J_1 + 36J_2 + 12J_3)M^2 \quad \text{(S2)}$$

$$E_{AFM1} = -(18J_1 + 36J_2 - 12J_3)M^2 \quad \text{(S3)}$$

$$E_{AFM2} = -(-18J_1 + 36J_2 + 0J_3)M^2 \quad \text{(S4)}$$

$$E_{AFM3} = -(-2J_1 - 12J_2 + 8J_3)M^2 \quad \text{(S5)}$$

Table S1. Calculated lattice parameters $a = b$ (Å), spontaneous out-of-plane polarization P (μC/cm^2) of $CuInP_2S_6$ monolayer and magnetic moment M (μ_B/Cr atom) of CrI_3 monolayer/bilayer. Previous theoretical and experimental results of $CuInP_2S_6$ and CrI_3 monolayer/bilayer are also provided for comparison.

	This work			DFT[1, 2]			Experiments[3-5]		
	$a = b$	P	M	$a = b$	P	M	$a = b$	P	M
$CuInP_2S_6$	6.13	5.45	—	6.126	5.35	—	6.10	3.8	—
Monolayer-CrI_3	6.98	—	3.47	6.85	—	3.15	6.87	—	3.1
Bilayer-CrI_3	6.98	—	—	6.92	—	—	6.87	—	—

Table S2. The optimized interlayer distance d (Å), binding energy E_b (meV), band gap E_g (eV) and the electrostatic potential difference $\Delta\varphi$ (eV) of the $CuInP_2S_6$/monolayer-CrI_3 and $CuInP_2S_6$/bilayer-CrI_3 heterostructures.

	d	E_b	E_g	$\Delta\varphi$
$CuInP_2S_6$-(P↑)/monolayer-CrI_3	3.54	-93.0	2.54	0.20
$CuInP_2S_6$-(P↓)/monolayer-CrI_3	3.56	-89.0	2.41	0.30
$CuInP_2S_6$-(P↑)/bilayer-CrI_3	3.55	-68.0	0.96	—
$CuInP_2S_6$-(P↓)/bilayer-CrI_3	3.58	-66.0	0.91	—

Table S3. The total energies of monolayer-CrI_3, bilayer-CrI_3, $CuInP_2S_6$/monolayer-CrI_3 and $CuInP_2S_6$/bilayer-CrI_3 heterostructures compared to FM state. The unit is meV/cell.

	FM	AFM1	AFM2	AFM3
Monolayer-CrI_3	0	138.1	179.2	138.4
Bilayer-CrI_3	0	-0.5	351.3	259.4
$CuInP_2S_6$-(P↑)/CrI_3	0	140.7	189.7	142.0
$CuInP_2S_6$-(P↓)/CrI_3	0	140.6	188.9	140.8
$CuInP_2S_6$-(P↑)/bilayer-CrI_3	0	-2.5	382.1	267.7
$CuInP_2S_6$-(P↓)/bilayer-CrI_3	0	1.5	382.6	269.7

Table S4. The total energies of $CuInP_2S_6$/monolayer-CrI_3 heterostructure in different interlayer distance *d* (Å) compared to FM state. The unit is meV/cell. P represents polarization direction.

d	P	FM	AFM1	AFM2	AFM3
2.8	P↑	0	151.79	229.34	157.34
	P↓	0	148.23	224.08	150.63
2.9	P↑	0	149.20	221.08	153.98
	P↓	0	146.98	216.91	148.23
3.0	P↑	0	147.14	213.86	151.09
	P↓	0	145.24	210.90	146.53
3.1	P↑	0	144.15	207.42	145.36
	P↓	0	143.89	205.20	144.84
3.2	P↑	0	142.98	202.23	143.98
	P↓	0	142.68	200.40	143.46
3.3	P↑	0	141.87	197.43	142.67
	P↓	0	141.83	196.42	142.47
3.4	P↑	0	141.16	193.99	141.82
	P↓	0	140.95	193.00	141.49

References

1. M. Zhao, G. Gou, X. Ding and J. Sun, *Nanoscale*, 2020, **12**, 12522-12530.
2. S. Tomar, B. Ghosh, S. Mardanya, P. Rastogi, B. Bhadoria, Y. S. Chauhan, A. Agarwal and S. Bhowmick, *Journal of Magnetism and Magnetic Materials*, 2019, **489**, 165384.
3. M. A. McGuire, H. Dixit, V. R. Cooper and B. C. Sales, *Chem. Mater*, 2015, **27**, 612-620.
4. F. Liu, L. You, K. L. Seyler, X. Li, P. Yu, J. Lin, X. Wang, J. Zhou, H. Wang and H. He, *Nature communications*, 2016, **7**, 1-6.
5. P. Jiang, C. Wang, D. Chen, Z. Zhong, Z. Yuan, Z.-Y. Lu and W. Ji, *Physical Review B*, 2019, **99**, 144401.